Cellular Signalling 63 (2019) 109384

Contents lists available at ScienceDirect

Cellular Signalling

journal homepage: www.elsevier.com/locate/cellsig

O-GlcNAcylated c-Jun antagonizes ferroptosis via inhibiting GSH synthesis in liver cancer

Yan Chen[a], Guoqing Zhu[a], Ya Liu[a], Qi Wu[a], Xiao Zhang[b], Zhixuan Bian[c], Yue Zhang[d], Qiuhui Pan[c,*], Fenyong Sun[a,*]

[a] Department of Clinical Laboratory Medicine, Shanghai Tenth People's Hospital of Tongji University, Shanghai 200072, China
[b] Shanghai Institute of Thoracic Tumors, Shanghai Chest Hospital, Shanghai Jiaotong University School of Medicine, Shanghai 200030, China
[c] Department of Laboratory Medicine, Shanghai Children's Medical Center, Shanghai Jiaotong University School of Medicine, Shanghai 200127, China
[d] Department of Central Laboratory, Shanghai Tenth People's Hospital of Tongji University, Shanghai 200072, China

ARTICLE INFO

Keywords:
Erastin
O-GlcNAcylation
Phosphorylation
Glutathione
Transcription
Promoter

ABSTRACT

Ferroptosis is a metabolism-related cell death. Stimulating ferroptosis in liver cancer cells is a strategy to treat liver cancer. However, how to eradicate liver cancer cells through ferroptosis and the obstacles to inducing ferroptosis in liver cancer remain unclear. Here, we observed that erastin suppressed the malignant phenotypes of liver cancer cells by inhibiting O-GlcNAcylation of c-Jun and further inhibited protein expression, transcription activity and nuclear accumulation of c-Jun. Overexpression of c-Jun-WT with simultaneous PuGNAc treatment conversely inhibited erastin-induced ferroptosis, whereas overexpression of c-Jun-WT alone or overexpression of c-Jun-S73A (a non-O-GlcNAcylated form of c-Jun) with PuGNAc treatment did not exert a similar effect. GSH downregulation induced by erastin was restored by overexpression of c-Jun-WT with simultaneous PuGNAc treatment. In addition, overexpression of c-Jun-WT, but not its S73A mutant, induced PSAT1 and CBS transcription via directly binding to their promoter regions, suggesting that GSH synthesis is regulated by O-GlcNAcylated c-Jun. A positive correlation between c-Jun O-GlcNAcylation and GSH was observed in clinical samples. Collectively, O-GlcNAcylated c-Jun represents an obstructive factor to ferroptosis, and targeting O-GlcNAcylated c-Jun might be helpful for treating liver cancer.

1. Introduction

The dynamic posttranslational modification O-linked β-*N*-acetylglucosamine glycosylation (O-GlcNAcylation), which is catalyzed by O-GlcNAc transferase (OGT), serves as a nutrient sensor to couple metabolic status to the stimulation of a variety of cancer promoting pathways [1,2]. In liver cancer, the core protein of the Hippo pathway, yes-associated protein (YAP), is O-GlcNAcylated by OGT at threonine (Thr) 241 and activates the glucose metabolism through stimulating the enzymes of the hexosamine biosynthetic pathway (HBP), nudix hydrolase 9 (NUDT9) and solute carrier family 5 member 3 (SLC5A3) [3]. The upstream factor of the O-GlcNAcylation-related signal is advanced glycosylation end product receptor (AGER). The AGER/OGT signal stimulates liver cancer accompanied by high glucose through the transcription factor c-Jun, which is O-GlcNAcylated at Serine (Ser) 73 [4]. In addition, other promoters in liver cancer, such as the receptor for activated C kinase 1 (RACK1) and histone deacetylase 1 (HDAC1), are O-GlcNAcylated to stimulate liver tumorigenesis [5,6]. However, most studies reported that O-GlcNAcylation stimulates liver tumorigenesis through HBP-related metabolism. Whether and how O-GlcNAcylation affects the occurrence and development of liver cancer through other mechanism remains unclear.

c-Jun is the first discovered oncogenic transcription factor [7]. In liver cancer, a clinical study in 2001 reported that the coordinated expression of c-Fos and c-Jun in HCC might reflect the coordinated tumor cell cycle of progression and proliferation [8]. c-Jun is initially important for liver cancer by antagonizing p53 activity to prevent apoptosis [9]. In addition, c-Jun promotes liver tumor cell survival during cancer initiation by regulating c-Fos- and SIRT6-dependent expression of survivin [10]. OCT4 and c-Jun bind to the promoters and stimulate the transcription of each other to expedite stemness of liver cancer cells [11]. Moreover, c-Jun promotes HBV-related liver tumorigenesis via targeting the dysplasia-associated cytokine, osteopontin, in transgenic mice [12]. We also validated the tumor-promoting role of c-Jun in previous studies. Mechanistically, c-Jun is activated by high-glucose-activated AGER/OGT signaling and reversely stimulates the

* Corresponding authors.
E-mail addresses: panqiuhui@263.net (Q. Pan), sunfenyongtongji@126.com (F. Sun).

https://doi.org/10.1016/j.cellsig.2019.109384
Received 22 April 2019; Received in revised form 23 July 2019; Accepted 3 August 2019
Available online 05 August 2019
0898-6568/

transcription of AGER via binding the JRE motif of the AGER promoter to form a positive feedback loop. The major O-GlcNAcylated site is the Ser73 of c-Jun [4]. However, how O-GlcNAcyalted c-Jun stimulates liver tumorigenesis must to be further investigated.

Ferroptosis, a form of regulated cell death first discovered in 2012, was originally found in cells exposed to the chemical compound erastin, which inhibited cystine uptake by the cystine/glutamate antiporter (system Xc^-), creating a void in the antioxidant defenses of the cell and ultimately leading to reactive oxygen species (ROS) accumulation-induced oxidative cell death [13–15]. Sorafenib, the only medical treatment with a proven efficacy against hepatocellular carcinoma, induces ferroptosis to eliminate liver tumor cells [16,17]. However, almost all patients develop sorafenib resistance within a few months [18]. We hypothesized that some factors or pathways might act as antagonists to reduce ferroptosis.

In this study, we observed that erastin specifically inhibited c-Jun O-GlcNAcylation in liver cancer and further suppressed the related cancer promoting function of c-Jun. However, overexpression of O-GlcNAcylated c-Jun conversely repressed ferroptosis via stimulating glutathione (GSH) synthesis through boosting the transcription of metabolic enzymes phosphoserine aminotransferases 1 (PSAT1) and cystathionine-beta-synthase (CBS). We also observed a positive association between O-GlcNAcylated c-Jun and GSH synthesis in clinical liver cancer samples. Inhibiting high level of O-GlcNAcylated c-Jun might represent a new strategy for liver cancer treatment.

2. Methods

2.1. Cell culture and vectors

Bel-7402 and SMMC-7721 were purchased from Cell Bank of the Chinese Academy of Sciences (Shanghai, China) and cultured in Dulbecco's Modified Eagled Medium (DMEM) with 10% fetal bovine serum. Erastin (Sigma, St Louis, MO, USA, 10 μM) with or without PuGNAc (Sigma, 25 μM), ferrostatin-1 (Sigma, 1 μM), ZVAD-FMK (Sigma, 10 μM) or necrosulfonamide (Sigma, 0.5 μM) were used to treat cell. The c-Jun-WT, c-Jun-S73A, c-Jun-sh1 and c-Jun-sh2 plasmids were obtained from our previous studies [4]. Promoter regions of WT- or Mutated (Mut)-*PSAT1* and *CBS* genes were amplified from gDNA of Bel-7402 cells and cloned into pGL4.21 (Promega, Madison, WI, USA) vectors. The primers used were listed in Supplementary Table 1.

2.2. Mouse experiments and tissue samples

Eight-week-old athymic nude mice were obtained from Bikai Laboratory Animal Crop (Bikai, Shanghai, China) and Bel-7402 cells (initial 5×10^6) were subcutaneously injected into each mouse. Dimethy sulfoxide (DMSO) or piperazine erastin (5 mg/kg, MedChemExpress, Monmouth Junction, NJ, USA) was subcutaneously injected once every day after xenografts were formed. The tumor volume was measured every 4 days and calculated as 0.5 x L x W^2, with L indicating length and W indicating width. Tumorous and adjacent liver tissues were acquired from the Shanghai Tenth People's Hospital under institutional approval. Informed written consent was obtained from all patients.

2.3. Immunofluorescence (IF), Western Blotting (WB) and Immunohistochemistry (IHC)

IF was performed as previously described [19], and the primary antibody used was anti-c-Jun [Cell Signaling Technology (CST), Boston, MA, #9165, monoclonal, Rabbit IgG, 1:200].

Subcellular extracts for WB were prepared using a kit from Active Motif (Carlsbad, CA, USA). WB was performed as previously described using primary antibodies: anti-c-PARP (Abcam, Hong Kong, China, #ab32064, monoclonal, Rabbit IgG, 1:1000), anti-p-MLKL (CST, #91689, monoclonal, Rabbit IgG, 1:1000), anti-ACSL4 (Abcam, #ab155282, monoclonal, Rabbit IgG, 1:1000), anti-c-Jun (CST, #9165, monoclonal, Rabbit IgG, 1:1000), anti-p-c-Jun (S73) (CST, #3270, monoclonal, Rabbit IgG, 1:1000), anti-GAPDH (CST, #5174, monoclonal, Rabbit IgG, 1:2000), anti-O-GlcNAc (Abcam, #ab2739, monoclonal, Mouse IgG, 1:1000), anti-HSP27 (Abcam, #ab5579, polyclonal, Rabbit IgG, 1:1000), anti-HDAC1 (Abcam, #ab7028, polyclonal, Rabbit IgG, 1:1000), anti-P27 (Abcam, #ab206927, monoclonal, Rabbit IgG, 1:1000), anti-RACK1 (Abcam, #ab62735, polyclonal, Rabbit IgG, 1:1000), anti-YB1 (Abcam, #ab12148, polyclonal, Rabbit IgG, 1:1000), anti-OGT (Abcam, #ab184198, monoclonal, Mouse IgG, 1:1000), anti-PSAT1 (Abcam, #ab96136, polyclonal, Rabbit IgG, 1:1000) and anti-CBS (Abcam, #ab96252, polyclonal, Rabbit IgG, 1:1000) [20].

IHC was performed as previously described using primary antibodies: anti-c-Jun (CST, #9165, monoclonal, Rabbit IgG, 1:200) and anti-p-c-Jun (S73) (CST, #3270, monoclonal, Rabbit IgG, 1:200) [3].

2.4. Luciferase reporter assay

Luciferase reporters were co-transfected into liver cancer cells with a Renilla luciferase expression plasmids. After incubation for 48 h, the cells were harvested and then lysed in the passive lysis buffer (Promega, Madison, WI, USA). Signals of luciferase reporters were then examined using dual-luciferase reagent (Promega).

2.5. Measurements of cell viability and colony formation

For the methylthiazol tetrazolium (MTT)-based cell viability assay, Bel-7402 and SMMC-7721 cells (3000 cells per well) were seeded in a 96-well plate, treated with 5 mg/ml MTT 5 days later, and lysed in DMSO after 4 h. Absorbance was measured at 595 nm. For soft agar colony formation assay, Bel-7402 and SMMC-7721 cells (6000 cells per well) were seeded in a 6-well plate of 0.3% agarose in DMEM media containing 10% FBS. Colonies from 12 fields of view were counted after 2 weeks.

2.6. Co-immunoprecipitation (co-IP)

Cells were washed using PBS and subsequently lysed in Western/IP lysis buffer (Beyotime, Haimen, China). Cells lysates were incubated with protein A/G magnetic beads (Novex, Oslo, Norway) overnight, washed five times and analyzed by WB. The antibodies used for immunoprecipitation were anti-O-GlcNAc (Abcam, #ab2739, monoclonal, Mouse IgG, 1:100), anti-OGT (Abcam, #ab177941, monoclonal, Rabbit IgG, 1:100 and #ab184198, monoclonal, Mouse IgG, 1:100), and anti-c-Jun (CST, #9165, monoclonal, Rabbit IgG, 1:100 and #2315, monoclonal, Mouse IgG, 1:100).

2.7. Enzymatic labelling of O-GlcNAc sites

In the first day, the co-immunoprecipitated protein complexes were added into reaction buffer (20 mM HEPES, pH 7.9, 50 mM NaCl, 1 mM PuGNAc, and 5 mM $MnCl_2$ with protease and phosphatase inhibitors). Gal-T1Y289L (Invitrogen, Carlsbad, CA, USA) and UDP-GalNAz (Invitrogen) were then added into reaction buffer. The mix was incubated overnight at 4 °C. In the second day, the beads were washed twice with reaction buffer, and the samples were reacted with biotin alkyne (Invitrogen) or tetramethyl-6-carboxyrhodamine (TAMRA) alkyne (Invitrogen). Finally, the biotin or TAMRA labeled proteins were analyzed by WB using anti-HRP-labeled-Streptavidin (Beyotime, #A0303, 1:2000) or anti-TAMRA (Invitrogen, #A6397, polyclonal, Rabbit IgG, 1:2000) antibodies [3].

2.8. Iron assay

The iron concentration in the cell lysates was assessed using an Iron

assay kit (Abcam). Cells were lysed in a Western/IP lysis buffer (Beyotime) at 4 °C for 20 min and centrifuged at 12,000 rpm for 15 min at 4 °C. Simultaneously, the standard curve was prepared using an iron standard that was diluted in ddH_2O. Iron assay buffer was added to samples before iron reducer was added. The standards and samples were then incubated at 25 °C for 30 min before the addition of iron probes and incubation in the dark at 25 °C for 60 min. The absorbance was finally measured at 593 nm using a microplate reader (Biotek, Winooski, VT, USA).

2.9. Lipid peroxidation assay

Malondialdehyde (MDA) concentrations in cell lysates were assessed using a lipid peroxidation assay kit (Abcam). The cells were lysed in lysis solution prepared by the manufacturer, homogenized on ice and centrifuged at 13,000 rpm for 10 min at 4 °C to collect the supernatant. Simultaneously, the standard curve was prepared using an MDA standard that was diluted in ddH_2O. Thiobarbituric acid (TBA) solution was then added to each sample. Next, the mixture was incubated at 95 °C for 60 min before adding it to a 96-well microplate. The absorbance was measured at 532 nm using a microplate reader (Biotek).

2.10. Glutathione assay

Glutathione (GSH) concentrations in cell lysates were assessed using a glutathione assay kit (Sigma). The standard curve was prepared using GSH standard diluted in an assay buffer. The cells were scraped and homogenized in PBS, deproteinized with 5% 5-sulfosalicylic acid and centrifuged to remove the protein precipitate. The supernatant was treated with 5, 5′–dithiobis (2–nitrobenzoic acid; DTNB). In principle, GSH reduces DTNB to 5-thio-2-nitrobenzoic acid (TNB) and oxidizes to glutathione disulfide (GSSG). Oxidized GSSG present in the cells reacts with the added NADPH to yield GSH, which subsequently reacts with DTNB to yield TNB. Thereby, total TNB indirectly reflects GSH concentration. The total TNB formed was finally measured by absorption at 412 nm in a microplate reader (Biotek).

2.11. Phospholipid assay

The phospholipid concentration in cell lysates was assessed using the phospholipid assay kit (Sigma). The standard curve was prepared using a phospholipid standard diluted in assay buffer. The cells were scraped and homogenized in assay buffer. Then, enzyme mix, phospholipase D (PLD) enzyme and dye reagent provided by the manufacturer were added per the instructions. The mixture was incubated for 30 min at room temperature without light. The absorbance was measured at 570 nm in a microplate reader (Biotek).

2.12. Glutamate assay

The phospholipid concentration in cell lysates was assessed using the glutamate assay kit (Sigma). The standard curve was prepared using a glutamate standard that was diluted in an assay buffer. Simultaneously, the cells were scraped and homogenized in the assay buffer. A glutamate developer and glutamate enzyme mix provided by the manufacturer were then added according to the instructions. The mix was incubated for 30 min at room temperature without light. The absorbance was measured at 450 nm with a microplate reader (Biotek).

2.13. Cysteine assay

The cysteine concentration in cell lysates was assessed using a cysteine assay kit (Sigma). The standard curve was prepared using the cysteine standard that was diluted in assay buffer. Simultaneously, the cells were scraped and homogenized in the assay buffer. Then, the diluted enzyme mix I, reducing agent, and homocysteine (HCY) blocker provided by the manufacturer were added per the recommended instructions. After incubation for 30 min at 37 °C, enzyme mix II was added to each reaction and then the mix was incubated for 5 min. A cysteine probe was added to each reaction, and fluorescence was measured using a microplate reader (Biotek).

2.14. Glycine assay

Glycine concentrations in cell lysates were assessed using the glycine assay kit (Sigma). The standard curve was prepared using the glycine standard that was diluted in ddH_2O. Simultaneously, the cells were scraped and homogenized in the assay buffer. Then, enzyme mix, developer and probe provided by the manufacturer were added per the recommended instructions. The mix was incubated for 60 min at 25 °C without light. Fluorescence was measured using a microplate reader (Biotek).

2.15. Enzyme-linked immunosorbent assay (ELISA)

The concentrations of cystathionine, serine, 3-PG, p-Pyr and p-Ser were evaluated by ELISA. The samples were diluted (1:4) in a dilution buffer provided by the manufacturer, and 50 μl of each diluted sample was added to 96-well microtiter plates for analysis. ELISA kits were purchased from Lichen Biotech Ltd. (Shanghai, China). ELISA assays were performed in strict accordance with the manufacturers' guidelines. The signals were determined by measuring the absorbance at 450 nm with a microplate reader (Biotek).

2.16. Protein ligation assay (PLA)

The PLA was performed to identify the direct interaction between two proteins using the Duolink™ in situ red starter kit (mouse/rabbit) (Sigma). The primary antibodies were anti-c-Jun (CST, #9165, monoclonal, Rabbit IgG, 1:200) and anti-O-GlcNAc (Abcam, Hongkong, China, #ab2739, monoclonal, Mouse IgG, 1:200). The detailed protocols were previously described [21].

2.17. Quantitative RT-PCR (qPCR)

The total RNA was extracted using Trizol, and the RNA was reverse-transcribed into complementary DNA using PrimeScript™ RT reagent Kit (Perfect Real Time) (TaKaRa, Dalian, China). qPCR was performed using a SYBR premix Ex Taq (TaKaRa) kit. The primers were listed in Supplementary table 1.

2.18. Chromatin immunoprecipitation (ChIP)

ChIP was performed using a kit from Active Motif (Carlsbad, CA, USA). The cells or samples were fixed using 1% formaldehyde, washed with PBS and lysed in a lysis buffer for sonication. Then, the protein-DNA complexes were incubated overnight with protein G beads (provided by the manufacturer) at 4 °C. The antibodies used for ChIP were anti-c-Jun (CST, #9165, monoclonal, Rabbit IgG, 1:100), anti-STAT3 (CST, #12640, monoclonal, Rabbit IgG, 1:100) and anti-IgG (CST, #3900, monoclonal, Rabbit IgG, 1:100). The DNA was eluted in 1% SDS/0.1 M NaHCO3, reversed cross-linked at 65 °C, purified by phenol/chloroform extraction and ethanol precipitation, and finally subjected to qPCR analysis [22].

2.19. Lipid ROS measurements

BODIPY-C11 (Invitrogen, D-3861) was added to a final concentration of 1.5 μM for 20 min before cells were harvested by trypsinization, washed and strained through a 40-μM cell strainer (BD Falcon, Franklin Lakes, NJ, USA). Cells were analyzed using a flow cytometer (BD FACSCanto II, BD Biosciences, San Jose, CA, USA) equipped with a 488-

nm laser for excitation. Data were collected from the FL1 channel with a minimum of 10,000 cells per sample.

2.20. Statistical analysis

Tests used to examine the differences between groups were one-way ANOVA and the Spearman rank-correlation analysis. A $P < .05$ was considered statistically significant.

3. Results

3.1. Malignant phenotypes of liver cancer cells are inhibited by ferroptosis inducer

C11-BODIPY is a fluorescent radio-probe for indexing lipid peroxidation and antioxidant efficacy in model membrane systems and living cells and is regarded as specific markers for ferroptosis [23,24]. We observed that erastin, a stimulator of ferroptosis, significantly upregulated C11-BODIPY fluorescence in two liver cancer cell lines, Bel-7402 and SMMC-7721, which demonstrated high carcinogenic properties in our previous studies [3,20]. The ferroptosis inhibitor ferrostatin-1 reversed erastin-induced upregulation of C11-BODIPY fluorescence, whereas ZVAD-FMK (the inhibitor for apoptosis) and necrosulfonamide (the inhibitor for necrosis) had no effect (Fig. 1A). Similarly, erastin positively regulated the concentration of another ferroptosis biomarker MDA [25]. This effect could be reversed by ferrostatin-1 but not by ZVAD-FMK and necrosulfonamide (Fig. 1B). Furthermore, erastin treatment significantly induced the expression of ACSL4, which is positively associated with ferroptosis levels [26,27]. Similarly, ferrostatin-1 restored, while ZVAD-FMK and necrosulfonamide did not affect erastin-induced upregulation of ACSL4 (Fig. 1B). We also found that erastin treatment had no effect on the expression of c-PARP (biomarker of apoptosis [28]) and p-MLKL (biomarker of necrosis [29,30]) (Fig. 1C). These data proved that erastin induces ferroptosis in liver cancer cells.

Next, we evaluated that whether stimulation of ferroptosis regulated malignant phenotypes of liver cancer cells. We observed that both cell viability and colony formation of liver cancer cells were inhibited by erastin treatment, whereas these effects were restored by simultaneous treatment of ferostatin-1 (Fig. 1D-1F). Moreover, simultaneous treatment of ZVAD-FMK or necrosulfonamide had no effect on erastin-induced suppression of cell viability and colony formation (Fig. 1D-1F). These results suggested that stimulation of ferroptosis inhibits the malignant phenotypes of liver cancer cells.

3.2. Cancer-promoting function of c-Jun is specifically inhibited by a ferroptosis inducer

Development of liver cancer is accompanied with increased O-GlcNAcylation levels [3,31]. We observed that erastin treatment significantly suppressed global O-GlcNAcylation levels in liver cancer cell lines Bel-7402 and SMMC-7721. These effects were reversed by simultaneous treatment with ferrostatin-1 but not affected by simultaneous treatment with ZVAD-FMK or necrosulfonamide (Fig. 2A). Previous studies have reported that oncoprotein c-Jun, HSP27, HDAC1, P27, RACK1 and YB1 are O-GlcNAcylated and promote liver cancer

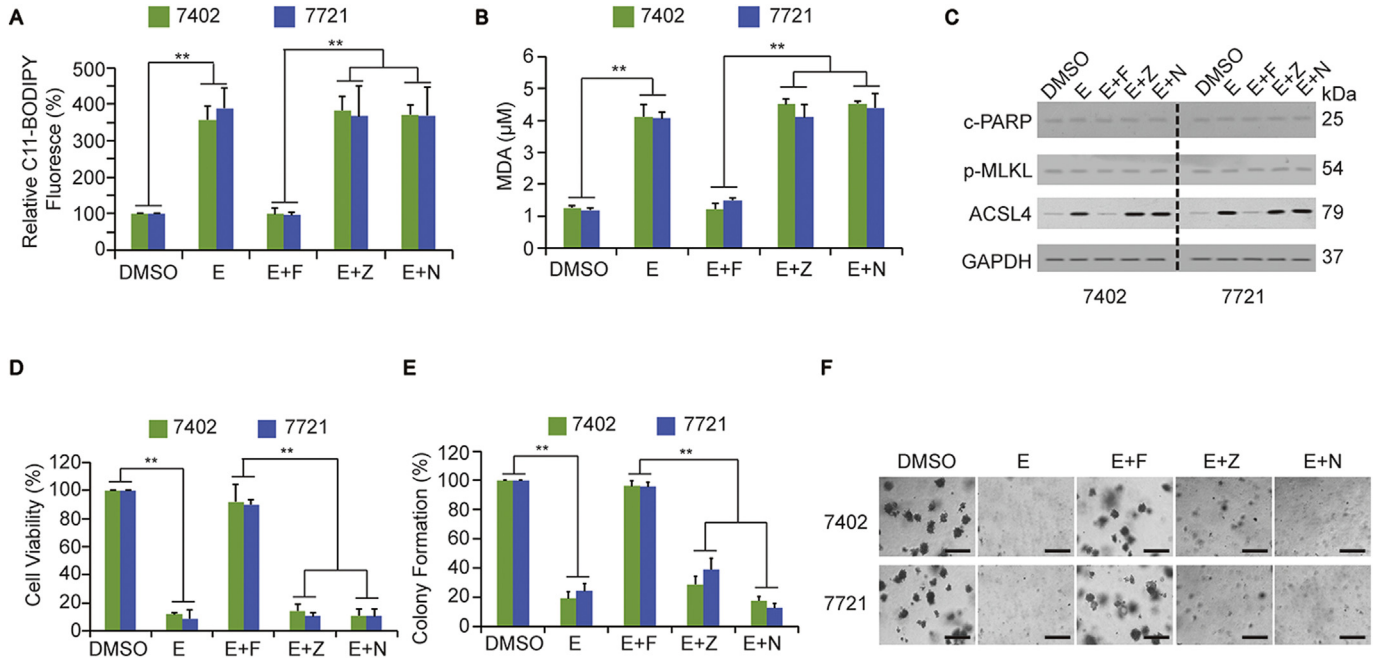

Fig. 1. Ferroptosis inhibits malignant phenotypes of liver cancer cells.
(A) Fluoresce of C11-BODIPY was measured in Bel-7402 and SMMC-7721 cells treated with DMSO or erastin with or without ferrostatin-1, ZVAD-FMK or necrosulfonamide (treatment time: 12 h).
(B) Concentrations of MDA was measured in Bel-7402 and SMMC-7721 cells treated with DMSO or erastin with or without ferrostatin-1, ZVAD-FMK or necrosulfonamide (treatment time: 12 h).
(C) Expression of c-PARP, p-MLKL or ACSL4 was measured by WB in Bel-7402 and SMMC-7721 cells treated with DMSO or erastin with or without ferrostatin-1, ZVAD-FMK or necrosulfonamide (treatment time: 12 h).
(D) Cell viability was measured using MTT-based assay in Bel-7402 and SMMC-7721 cells treated with DMSO or erastin with or without ferrostatin-1, ZVAD-FMK or necrosulfonamide (treatment time: 12 h).
(*E*-F) Colony formation was measured using soft agar colony formation assay in Bel-7402 and SMMC-7721 cells treated with DMSO or erastin with or without ferrostatin-1, ZVAD-FMK or necrosulfonamide (treatment time: 12 h). Scale bar, 200 μm.
The data are presented as the means ± SD from three biological replicates. **, $p < .01$. The data shown in (A), (B), (D) and (E) were analyzed using a one-way ANOVA test. E, erastin; F, ferrostatin-1; Z, ZVAD-FMK; N, necrosulfonamide.

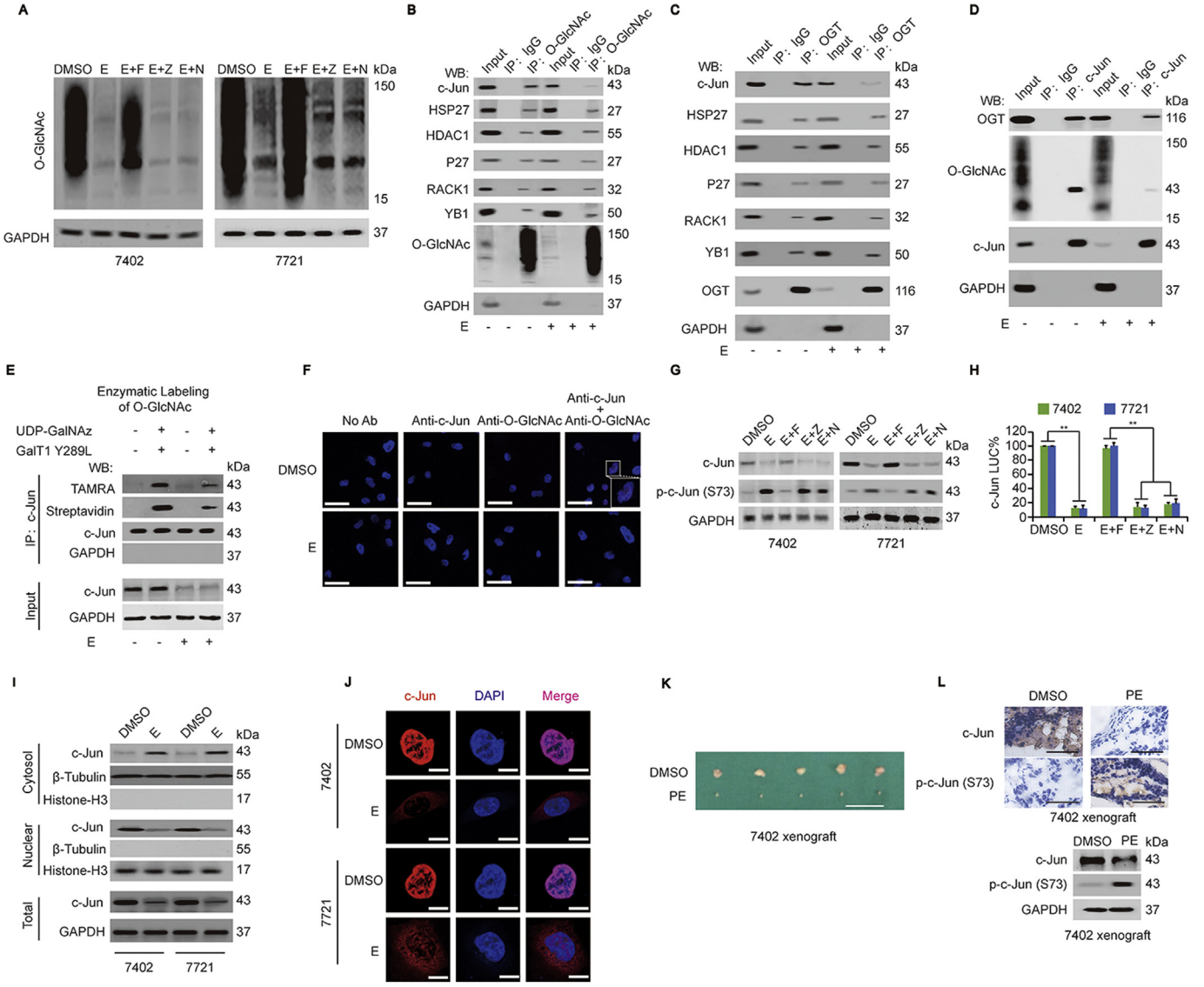

Fig. 2. Ferroptosis inhibits c-Jun activity.

(A) Global O-GlcNAcylation level was measured by WB in Bel-7402 and SMMC-7721 cells treated with DMSO or erastin with or without ferrostatin-1, ZVAD-FMK or necrosulfonamide (treatment time: 12 h).

(B-D) Proteins were immunocipitated by anti-O-GlcNAc (B), OGT (C), or c-Jun (D) antibodies with or without erastin treatment, and co-immunoprecipitated proteins were detected using indicated antibodies in Bel-7402 cells, the erastin treatment time was 24 h (B), 24 h (C) and 8 h (D), respectively. The O-GlcNAc (B), OGT (C) and c-Jun (D) level in the co-IP samples were adjusted to the same content.

(E) Endogenous c-Jun was immunoprecipitated by anti-c-Jun antibodies in Bel-7402 cells treated with or without UDP-GalNAz, GalT1 Y289L or erastin as indicated (treatment time: 12 h). The biotin or TAMRA labeled O-GlcNAcylated c-Jun was measured by anti-Streptavidin or anti-TAMRA. The c-Jun level in each co-IP samples were adjusted to the same content.

(F) The interaction between c-Jun and O-GlcNAc was measured using PLA in Bel-7402 cells with DMSO or erastin treatment (treatment time: 12 h). The areas with red signals were enlarged by a square. Scale bar, 200 μm.

(G) c-Jun and phosphorylation of Ser73 at c-Jun were measured by WB in in Bel-7402 and SMMC-7721 cells treated with DMSO or erastin with or without ferrostatin-1, ZVAD-FMK or necrosulfonamide (treatment time: 12 h).

(H) Luciferase activity of c-Jun pathway was measured using a luciferase reporter assay in Bel-7402 and SMMC-7721 cells treated with DMSO or erastin with or without ferrostatin-1, ZVAD-FMK or necrosulfonamide (treatment time: 12 h).

(I) The nuclear and cytosol components of Bel-7402 and SMMC-7721 cells treated with or without erastin were extracted. The levels of c-Jun were subsequently examined by WB.

(J) Subcellular distribution of c-Jun in Bel-7402 and SMMC-7721 cells treated with or without erastin (treatment time: 12 h) was by a confocal microscopy assay. Scale Bar, 50 μm.

(K-L) Xenografts formed by Bel-7402 cells treated with or without piperazine erastin was shown (L). Expression of c-Jun and phosphorylation of Ser73 at c-Jun were subsequently measured by IHC and WB, respectively (L). Scale bar, 1 cm.

The data are presented as the means ± SD from three biological replicates. **, $p < .01$. The data shown in (H) were analyzed using a one-way ANOVA test. E, erastin; F, ferrostatin-1; Z, ZVAD-FMK; N, necrosulfonamide; PE, piperazine erastin. (For interpretation of the references to colour in this figure legend, the reader is referred to the web version of this article.)

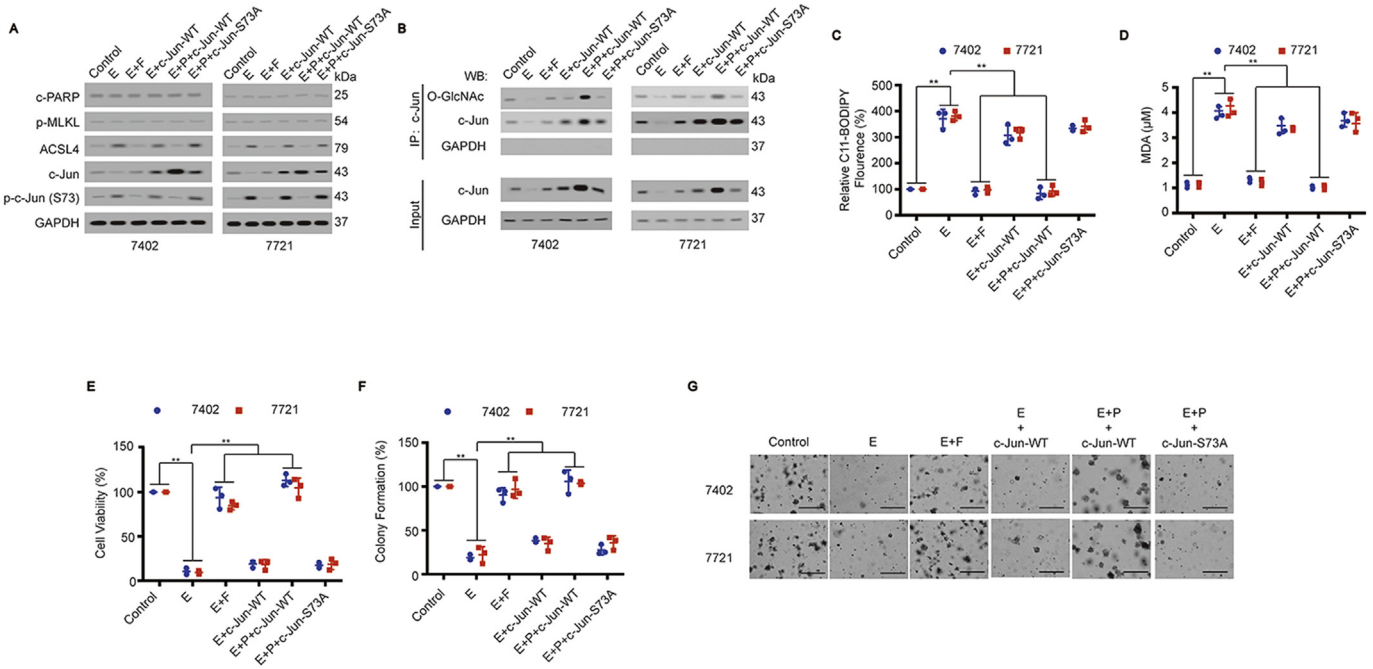

Fig. 3. Ser73 O-GlcNAc modified c-Jun inhibits ferroptosis.

(A) Bel-7402 and SMMC-7721 cells were treated as indicated (drug treatment time: 12 h). Expression of indicated proteins were subsequently measured using WB.

(B) c-Jun was immunoprecipitated using anti-c-Jun antibodies in Bel-7402 and SMMC-7721 with indicated treatment (drug treatment time: 12 h), and the levels of c-Jun in each co-IP samples were adjusted to the same contents. O-GlcNAc levels were then measured by WB.

(C) Fluoresce of C11-BODIPY was measured in Bel-7402 and SMMC-7721 cells with indicated treatment (drug treatment time: 12 h).

(D) Concentrations of MDA was measured in Bel-7402 and SMMC-7721 cells with indicated treatment (drug treatment time: 12 h).

(*E*-G) Cell viability (E) and colony formation (F-G) of Bel-7402 and SMMC-7721 cells with indicated treatment (drug treatment time: 12 h) were measured. The represented images of cell colonies were shown in G. Scale bar, 200 μm.

The data are presented as the means ± SD from three biological replicates. **, $p < .01$. The data shown in (C−F) were analyzed using a one-way ANOVA test. E, erastin; F, ferrostatin-1, P, PuGNAc.

development [4–6,32–34]. We performed co-immunoprecipitation experiments in Bel-7402 cells and observed that erastin significantly inhibited the bindings of c-Jun to O-GlcNAc and OGT (Fig. 2B and C). However, bindings of other oncoproteins (HSP27, HDAC1, P27, RACK1 and YB1) to O-GlcNAc or OGT were not obviously influenced by erastin in contrast to the findings for c-Jun (Fig. 2B and C). Additionally, OGT or O-GlcNAc binding to c-Jun was significantly inhibited by erastin treatment in Bel-7402 cells (Fig. 2D). Enzymatic labeling of O-GlcNAc experiments further validated that O-GlcNAcylation of c-Jun were inhibited erastin treatment (Fig. 2E). Moreover, protein ligation assay results suggested that erastin restrained the originally obvious interaction between c-Jun and O-GlcNAc in Bel-7402 cells (Fig. 2F). These results demonstrated that ferroptosis inhibits O-GlcNAcylation of c-Jun without affecting O-GlcNAcylation of other previously reported O-GlcNAcylated oncoproteins.

We next investigated whether other cancer-promoting functions of c-Jun, such as protein expression, phosphorylation, transcription activity and intracellular distribution, are regulated when ferroptosis is induced. First, we found that erastin significantly inhibited c-Jun expression. This effect was reversed by ferrostatin-1 treatment but not influenced by ZVAD-FMK or necrosulfonamide treatment in both Bel-7402 and SMMC-7721 cells (Fig. 2G). Interestingly, the phosphorylation level of Ser73 at c-Jun (negatively associated with the c-Jun activity [4]) was stimulated after erastin treatment in both Bel-7402 and SMMC-7721 cells (Fig. 2G). Erastin treatment also inhibited luciferase activity of c-Jun transcription compared to control treatment, and this effect could be reversed by ferrostatin-1 but not influenced by ZVAD-FMK or necrosulfonamide (Fig. 2H), These results suggest that ferroptosis inhibited protein expression and activity and stimulated c-Jun phosphorylation.

c-Jun mainly performed its oncogenic role in the nucleus to stimulate downstream transcription [4,35]. We observed that erastin treatment slightly induced cytosol expression but significantly inhibited nuclear expression of c-Jun in both Bel-7402 and SMMC-7721 cells (Fig. 2I). Moreover, c-Jun was translocated from nucleus to cytoplasm after erastin treatment in both Bel-7402 and SMMC-7721 cells (Fig. 2J), suggesting that the ferroptosis stimulus erastin suppresses the oncogenic function of c-Jun. Additionally, piperazine erastin (a more stable erastin in vivo) treatment reduced the volume of xenografts formed by Bel-7402 cells (Fig. 2K). We observed that piperazine erastin negatively regulated expression of c-Jun but positively regulated the phosphorylation of Ser73 in c-Jun in xenografts formed by Bel-7402 cells (Fig. 2L). These data demonstrated that ferroptosis inhibited the cancer-promoting functions of c-Jun both in vitro and in vivo.

3.3. O-GlcNAcylated c-Jun prevents resist ferroptosis in liver cancer cells

Ser73 in c-Jun is the major O-GlcNAcylation site in liver cancer cells [4]. We observed that overexpression of c-Jun-Wild type (WT) with simultaneous PuGNAc treatment (the stimulus of O-GlcNAcylation) reversed erastin-induced upregulation of ACSL4, whereas overexpression of c-Jun-WT alone or overexpression of c-Jun-S73A with simultaneous PuGNAc treatment did not influence ACSL4 expression (Fig. 3A). Additionally, we observed that overexpression of c-Jun-WT with simultaneous PuGNAc treatment inhibited erastin-induced increases in phosphorylated c-Jun, whereas overexpression of c-Jun-WT or c-Jun-S73A (a non-O-GlcNAcylated form of c-Jun) did not influence the erastin-induced increase in phosphorylated c-Jun (Fig. 3A). However, overexpression of c-Jun-WT with simultaneous PuGNAc treatment reversed erastin-induced reduction of O-GlcNAcylated c-Jun, whereas overexpression of c-Jun-WT alone or overexpression of c-Jun-S73A with simultaneous PuGNAc treatment did not have a similar effect (Fig. 3B).

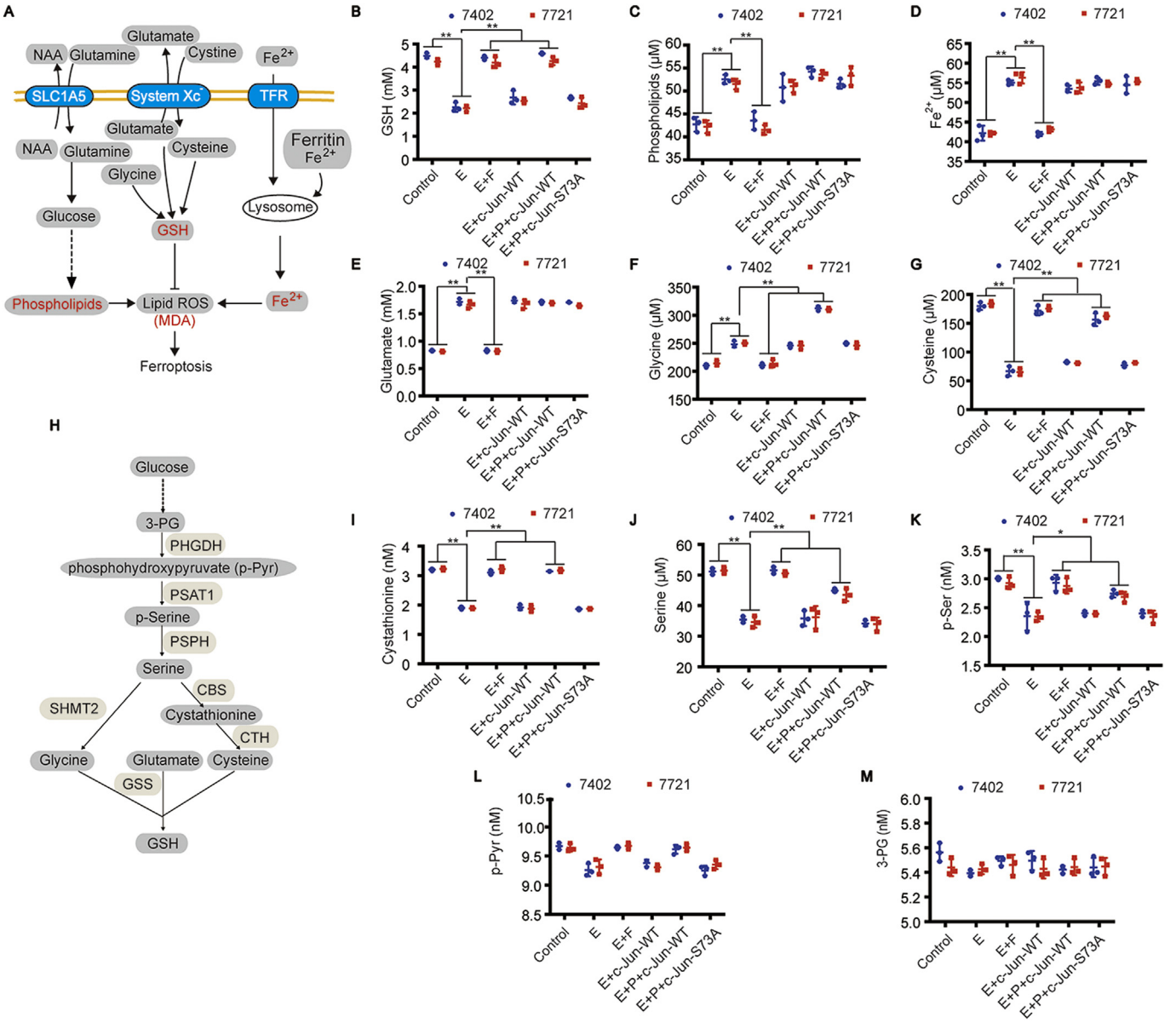

Fig. 4. Ser73 O-GlcNAc modified c-Jun inhibits GSH synthesis.
(A) Schematic presentation of metabolic pathways that affect lipid ROS to cause ferroptosis.
(B-G) Concentrations of GSH, phospholipids, Fe2+, glutamate, glycine and cysteine in Bel-7402 and SMMC-7721 cells with indicated treatment (drug treatment time: 12 h).
(H) Schematic presentation of metabolic pathways from Glucose to GSH.
(I-M) Concentrations of cystathionine, serine, p-Ser, p-Pyr and 3-PG in Bel-7402 and SMMC-7721 cells with indicated treatment (drug treatment time: 12 h).
The data are presented as the means ± SD from three biological replicates. *, $p < .05$, **, $p < .01$. The data shown in (B-G and I-M) were analyzed using a one-way ANOVA test. E, erastin; F, ferrostatin-1.

We also found that overexpression of c-Jun-WT with simultaneous PuGNAc treatment restored erastin-induced upregulation of C11-BODIPY fluorescence and MDA concentrations, whereas overexpression of c-Jun-WT alone or overexpression of c-Jun-S73A with simultaneous PuGNAc treatment did not have a similar effect (Fig. 3C-D). Finally, we observed that overexpression of c-Jun-WT with simultaneous PuGNAc treatment did not invert erastin-induced suppression of cell viability and colony formation, whereas overexpression of c-Jun-WT alone or overexpression of c-Jun-S73A with simultaneous PuGNAc treatment did not exhibit an analogous function (Fig. 3E-3G). These data suggested that increasing amount of O-GlcNAcylated c-Jun could block ferroptosis and reverse ferroptosis-related inhibition of malignant phenotypes of liver cancer cells.

Additionally, we evaluated whether PuGNAc alone regulates ferroptosis, or has the ability to reverse erastin-induced ferroptosis. We observed that PuGNAc alone did not significantly regulate the ferroptosis markers C11-BODIPY, MDA and ACSL4 and could not reverse erastin-induced upregulation of C11-BODIPY fluorescence, MDA concentration and ACSL4 expression (Supplementary Fig. 1A-C), whereas PuGNAc alone promoted cell viability and colony formation in Bel-7402 and SMMC-7721 cells (Supplementary Fig. 1D-F). Therefore, PuGNAc might promote the malignant phenotypes of liver cancer cells in a ferroptosis- independent manner.

3.4. O-GlcNAcylated c-Jun stimulates GSH synthesis pathway

Ferroptosis is promoted by increased of lipid ROS, and at least three metabolites regulate the synthesis of lipid ROS. Phospholipids and Fe^{2+}

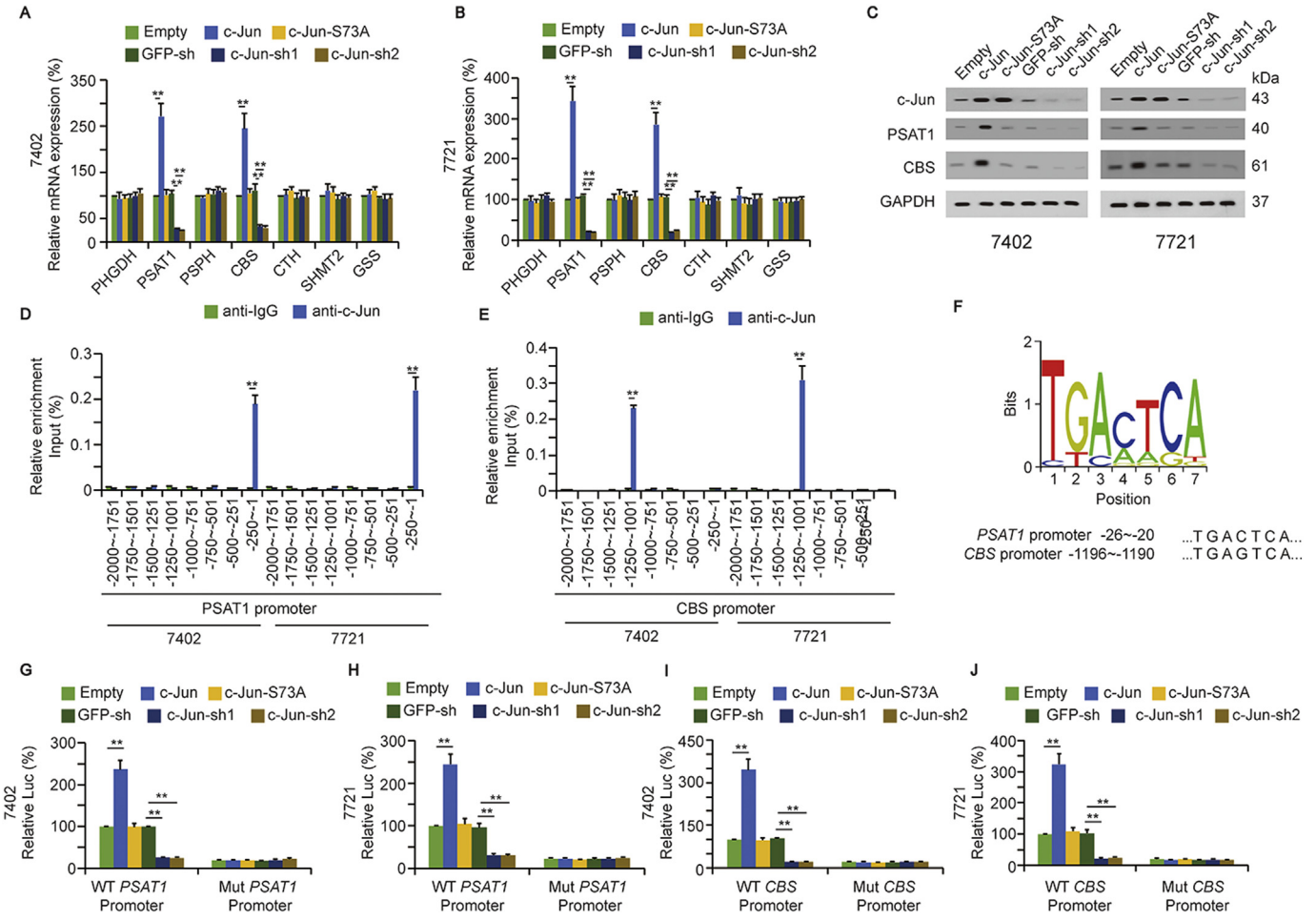

Fig. 5. Ser73 O-GlcNAc modified c-Jun inhibits the transcription of PSAT1 and CBS.

(A-B) c-Jun-WT, c-Jun-S73A, c-Jun-sh1 or c-Jun-sh2 plasmids were transfected into Bel-7402 (A) or SMMC-7721 cells (B), and the mRNA levels of PHGDH, PSAT1, PSPH, CBS, CTH, SHMT2 and GSS were detected using qPCR.

(C) c-Jun-WT, c-Jun-S73A, c-Jun-sh1 or c-Jun-sh2 plasmids were transfected into Bel-7402 and SMMC-7721 cells. The protein levels of c-Jun, PSAT1 and CBS were detected using WB.

(D-E) The enrichment of c-Jun in Bel-7402 and SMMC-7721 cells at indicated regions of indicated PSAT1 and CBS promoter was calculated as the percentage of input chromosomal DNA via ChIP using the corresponding antibodies. A non-specific IgG was used as the negative control antibody.

(F) c-Jun binding motif from JASPAR database was identified in *PSAT1* and *CBS* promoter.

(G-H) c-Jun-WT, c-Jun-S73A, c-Jun-sh1 or c-Jun-sh2 plasmids were transfected into Bel-7402 (G) and SMMC-7721 cells (H). Luciferase activities of WT- or Mut-*PSAT1* promoter were detected using the dual-luciferase regent.

(I-J) c-Jun-WT, c-Jun-S73A, c-Jun-sh1 or c-Jun-sh2 plasmids were transfected into Bel-7402 (I) and SMMC-7721 cells (J). Luciferase activities of WT- or Mut- *CBS* promoter were detected using the dual-luciferase regent.

The data are presented as the means ± SD from three biological replicates. *, $p < .05$, **, $p < .01$. The data shown in (A-B, D-E and G-J) were analyzed using a one-way ANOVA test.

upregulate lipid ROS, whereas GSH downregulates lipid ROS (Fig. 4A) [13,36,37]. We observed that erastin treatment significantly inhibited of GSH concentrations and increased phospholipids and Fe^{2+} concentrations (Fig. 4B-4D). However, only GSH downregulation induced by erastin could be reversed by overexpression of c-Jun-WT with simultaneous PuGNAc treatment, and phospholipids and Fe^{2+} upregulation induced by erastin could not be reversed by overexpression of c-Jun-WT with simultaneous PuGNAc treatment (Fig. 4B-4D). In addition, overexpression of c-Jun-WT alone or overexpression of c-Jun-S73A with simultaneous PuGNAc treatment did not influence the concentration changes of these three metabolites induced by erastin (Fig. 4B-4D). These results suggested that O-GlcNAcylated c-Jun resists ferroptosis via stimulates GSH synthesis without regulating phospholipids and Fe^{2+}.

GSH is synthesized by glutamate, cysteine and glycine [38]. We observed that erastin treatment upregulated the concentrations of glutamate and glycine but downregulated the cysteine concentrations. Moreover, overexpression of c-Jun-WT with simultaneous treatment of PuGNAc reversed the downregulation of cysteine concentration induced by erastin treatment and further upregulated the concentration of glycine without influencing the concentration of glutamate (Fig. 4E-4G). Both cysteine and glycine are synthesized by the pathway from glucose to serine [39] (Fig. 4H). Thus, we next investigated whether O-GlcNAcylated c-Jun upregulates the concentration of glycine and cysteine generated from this pathway. We observed that erastin treatment could inhibit the concentrations of cystathionine, serine and p-Ser, whereas overexpression of c-Jun-WT with simultaneous PuGNAc treatment reversed these effects (Fig. 4I-4K). Moreover, the upstream metabolites p-Pyr and 3-PG were not influenced by erastin treatment or simultaneous overexpression of c-Jun with PuGNAc treatment (Fig. 4L and M). These results demonstrated that the metabolite pathway from p-Ser to GSH is stimulated by O-GlcNAcylated c-Jun.

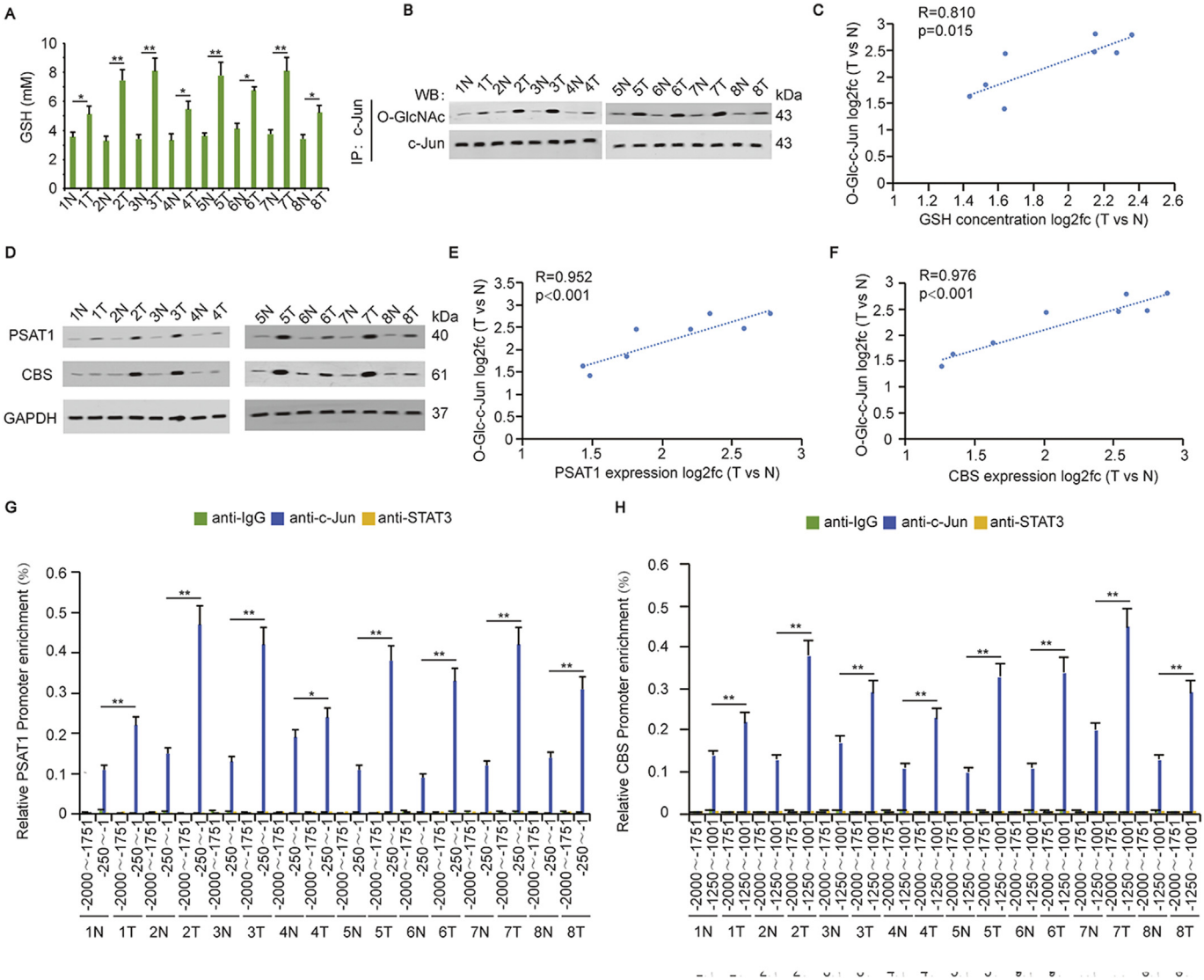

Fig. 6. O-GlcNAc modified c-Jun was positively associated with GSH related pathway in clinical samples.
(A) GSH concentration was detected in tumor and adjacent normal tissues.
(B) c-Jun was immunoprecipitated using anti-c-Jun antibodies, and the co-immunoprecipitated O-GlcNAc was detected using WB.
(C) Relationship between O-GlcNAclated c-Jun and GSH concentration was analyzed.
(D) PSAT1 and CBS expression were detected using WB in clinical samples.
(E-F) Relationship between O-GlcNAclated c-Jun and PSAT1 (E) or CBS (F) expression was analyzed.
(G-H) The enrichment of c-Jun or STAT3 in tumor or adjacent normal tissues at indicated regions of PSAT1 or CBS was detected using ChIP. A non-specific IgG was used as the negative control antibody.
The data are presented as the means ± SD from three biological replicates. *, $p < .05$, **, $p < .01$. The data shown in (A, G and H) were analyzed using a one-way ANOVA test. The data shown in (C, E and F) were analyzed using the Spearman rank-correlation analysis.

3.5. O-GlcNAcylated c-Jun stimulates PSAT1 and CBS transcription

We next investigated whether c-Jun stimulates the transcription of enzymes in the GSH synthesis pathway. We observed that overexpression of c-Jun-WT induced phosphoserine aminotransferase 1 (PSAT1) and cystathionine β synthase (CBS) mRNA levels, whereas overexpression of c-Jun-S73A did not regulate the mRNA levels of these two enzymes in Bel-7402 and SMMC-7721 cells. Knockdown of c-Jun inhibited PSAT1 and CBS mRNA levels. Additionally, overexpression or knockdown of c-Jun did not influence the mRNA levels of other enzymes in the metabolite pathway from 3-PG to GSH (Fig. 5A and B). We also performed Western blots experiments and observed that overexpression of c-Jun-WT induced PSAT1 and CBS protein expression, while overexpression of c-Jun-S73A did not exert a similar effect. Knockdown of c-Jun inhibited PSAT1 and CBS protein levels in Bel-7402 and SMMC-7721 cells (Fig. 5C). ChIP experiments revealed that c-Jun directly bound to the −250~ − 1 promoter region of *PSAT1* and the −1250~ − 1001 promoter region of *CBS* (Fig. 5D-E). Moreover, the c-Jun binding motifs (TGACTCA/TGAGTCA, from JASPAR database) were identified in the −26~ − 20 promoter region of *PSAT1* and the −1196~ − 1190 promoter region of *CBS* (Fig. 5F). We constructed WT and motif-mutant promoter luciferase reporters and found that overexpression of c-Jun-WT could significantly induce the luciferase activities of WT-*PSAT1* and *CBS* promoters. In contrast, overexpression of c-Jun-S73A did not have a similar effect, and knockdown of c-Jun inhibited the luciferase activities of the WT-*PSAT1* and *CBS* promoters in both Bel-7402 and SMMC-7721 cells. However, overexpression of c-Jun-WT/S73A or knockdown of c-Jun had no obvious regulatory effect on the luciferase activities of Mut-*PSAT1* and *CBS* promoter (Fig. 5G–5J). These results demonstrated that O-GlcNAcylated c-Jun

stimulates transcription of PSAT1 and CBS via directly binding their promoters.

3.6. O-GlcNAcylated c-Jun is positively associated with the GSH synthesis in clinical samples

Eight pairs of liver cancer and adjacent normal tissue samples were acquired, and we observed that GSH concentrations and O-GlcNAcylated c-Jun were upregulated in liver cancer tissues compared to adjacent normal tissues (Fig. 6A and B). A positive correlation was identified for the fold-change (tumor vs. normal) between GSH concentration and level of O-GlcNAcylated c-Jun ($R = 0.810$, $p = .015$) (Fig. 6C). We also observed that PSAT1 and CBS were highly expressed in liver cancer tissues compared with adjacent normal tissues (Fig. 6D). Positive correlations between O-GlcNAcylated c-Jun levels and PSAT1 expression ($R = 0.952$, $p < .001$) as well as CBS expression ($R = 0.976$, $p < .001$) were also observed (Fig. 6E and F). ChIP-qPCR was performed using the primers designed for the $-2000\sim-1751$ or $-250\sim-1$ regions of the *PSAT1* promoter and the $-2000\sim-1751$ or $-1250\sim-1001$ regions of the *CBS* promoter for the eight paired of clinical samples. We found that c-Jun binds to the $-250\sim-1$ region of the *PSAT1* promoter but $-1250\sim-1001$ region of the *CBS* promoter but could not bind with the $-2000\sim-1751$ regions of the *PSAT1* and *CBS* promoters. Moreover, IgG and STAT3 did not bind to these regions of the *PSAT1* and *CBS* promoters (Fig. 6G and H). These data suggested the positive correlation between O-GlcNAcylated c-Jun and synthesis pathways in clinical samples.

4. Discussion

Ferroptosis is a form of metabolism-related programmed cell death and results from ROS accumulation. Previous studies of liver cancer have reported that the transcription factor nuclear factor erythroid 2 like 2 (NRF2) inhibits ROS accumulation by activating the expression of a series of reductases, and metallothionein (MT)-1G inhibits GSH depletion and lipid peroxidation to inhibit the potential ferroptosis [17,40]. However, how ferroptosis exerts its role in the eradication of liver cancer cells was not previously reported. Here, we found that ferroptosis inhibits the global O-GlcNAcylation of liver cancer cells, especially the O-GlcNAcylation of c-Jun. Further, the tumor promotion function of c-Jun such as transcription activity and nuclear accumulation was inhibited. These finding provide new evidences and elucidate the possible mechanisms by which ferroptosis inhibits liver tumorigenesis.

Sorafenib is the only medical treatment with proven efficacy against hepatocellular carcinoma and eliminates tumor cells via ferroptois [16,17]. However, almost all patients develop sorafenib resistance within a few months [18]. Activation of c-Jun is associated with resistance to sorafenib and poor overall survival and inhibits sorafenib-induced cell death [41,42]. Here, we observed that O-GlcNAcylated c-Jun stimulated GSH synthesis via increasing PSAT1 and CBS transcription to inhibit ferroptosis. Therefore, we hypothesized O-GlcNAcylated c-Jun stimulates GSH synthesis to inhibit sorafenib-induced ferroptosis and induce sorafenib resistance in liver cancer. Inhibiting O-GlcNAcylation and c-Jun expression might provide new strategies in liver cancer treatment, especially ferroptosis-related treatment.

Previous studies have reported that c-Jun is a regulator of glucose metabolism. c-Jun activates HBP via binding the promoter of the HBP upstream stimulator AGER [4]. Moreover, c-Jun is also promoted glutamine and the TCA cycle via stimulating mitochondrial glutaminase levels [43]. In this study, we found that c-Jun stimulated GSH synthesis via increasing PSAT1 and CBS transcription. Moreover, the c-Jun binding motif was identified in PSAT1 and CBS promoters. The positive relationship between c-Jun and GSH synthesis was also identified in clinical liver cancer tissues. However, whether c-Jun stimulates other metabolic pathways requires further investigation.

Collectively, we reported that induction of ferroptosis could suppress liver tumorigenesis via inhibiting c-Jun O-GlcNAcylation. Importantly, overexpression of O-GlcNAcylated c-Jun exerted an inhibitory role on ferroptosis via inhibiting GSH synthesis. Blocking c-Jun O-GlcNAcylation might be helpful for ferroptosis-related treatment of HCC.

Declaration of Competing Interest

The authors declare no conflict of interest.

Acknowledgement

This study was supported by the National Natural Science Foundation of China (81601829, 81702741, 81772941 and 81871727), “Chen Guang” project supported by Shanghai Municipal Education Commission and Shanghai Education Development Foundation (Grant 18CG16), Shanghai Sailing Program (19YF1444800), and Nurture projects for basic research of Shanghai Chest Hospital (2018YNJCQ06).

Appendix A. Supplementary data

Supplementary data to this article can be found online at https://doi.org/10.1016/j.cellsig.2019.109384.

References

[1] W. Yi, P.M. Clark, D.E. Mason, M.C. Keenan, C. Hill, W.A. Goddard 3rd, E.C. Peters, E.M. Driggers, L.C. Hsieh-Wilson, Phosphofructokinase 1 glycosylation regulates cell growth and metabolism, Science 337 (6097) (2012) 975–980.
[2] C. Slawson, G.W. Hart, O-GlcNAc signalling: implications for cancer cell biology, Nat. Rev. Cancer 11 (9) (2011) 678–684.
[3] X. Zhang, Y. Qiao, Q. Wu, Y. Chen, S. Zou, X. Liu, G. Zhu, Y. Zhao, Y. Chen, Y. Yu, Q. Pan, J. Wang, F. Sun, The essential role of YAP O-GlcNAcylation in high-glucose-stimulated liver tumorigenesis, Nat. Commun. 8 (2017) 15280.
[4] Y. Qiao, X. Zhang, Y. Zhang, Y. Wang, Y. Xu, X. Liu, F. Sun, J. Wang, High glucose stimulates tumorigenesis in hepatocellular carcinoma cells through AGER-dependent O-GlcNAcylation of c-Jun, Diabetes 65 (3) (2016) 619–632.
[5] G. Zhu, T. Tao, D. Zhang, X. Liu, H. Qiu, L. Han, Z. Xu, Y. Xiao, C. Cheng, A. Shen, O-GlcNAcylation of histone deacetylases 1 in hepatocellular carcinoma promotes cancer progression, Glycobiology 26 (8) (2016) 820–833.
[6] F. Duan, H. Wu, D. Jia, W. Wu, S. Ren, L. Wang, S. Song, X. Guo, F. Liu, Y. Ruan, J. Gu, O-GlcNAcylation of RACK1 promotes hepatocellular carcinogenesis, J. Hepatol. 68 (6) (2018) 1191–1202.
[7] P.K. Vogt, Fortuitous convergences: the beginnings of JUN, Nat. Rev. Cancer 2 (6) (2002) 465–469.
[8] M.F. Yuen, P.C. Wu, V.C. Lai, J.Y. Lau, C.L. Lai, Expression of c-Myc, c-Fos, and c-Jun in hepatocellular carcinoma, Cancer 91 (1) (2001) 106–112.
[9] R. Eferl, R. Ricci, L. Kenner, R. Zenz, J.P. David, M. Rath, E.F. Wagner, Liver tumor development. c-Jun antagonizes the proapoptotic activity of p53, Cell 112 (2) (2003) 181–192.
[10] L. Min, Y. Ji, L. Bakiri, Z. Qiu, J. Cen, X. Chen, L. Chen, H. Scheuch, H. Zheng, L. Qin, K. Zatloukal, L. Hui, E.F. Wagner, Liver cancer initiation is controlled by AP-1 through SIRT6-dependent inhibition of survivin, Nat. Cell Biol. 14 (11) (2012) 1203–1211.
[11] K.K. Kuo, K.T. Lee, K.K. Chen, Y.H. Yang, Y.C. Lin, M.H. Tsai, K. Wuputra, Y.L. Lee, C.C. Ku, H. Miyoshi, Y. Nakamura, S. Saito, C.C. Wu, C.Y. Chai, R. Eckner, C.L. Steve Lin, S.S. Wang, D.C. Wu, C.S. Lin, K.K. Yokoyama, Positive feedback loop of OCT4 and c-JUN expedites Cancer Stemness in liver Cancer, Stem Cells 34 (11) (2016) 2613–2624.
[12] C. Trierweiler, B. Hockenjos, K. Zatloukal, R. Thimme, H.E. Blum, E.F. Wagner, P. Hasselblatt, The transcription factor c-JUN/AP-1 promotes HBV-related liver tumorigenesis in mice, Cell Death Differ. 23 (4) (2016) 576–582.
[13] S.J. Dixon, K.M. Lemberg, M.R. Lamprecht, R. Skouta, E.M. Zaitsev, C.E. Gleason, D.N. Patel, A.J. Bauer, A.M. Cantley, W.S. Yang, B. Morrison 3rd, B.R. Stockwell, Ferroptosis: an iron-dependent form of nonapoptotic cell death, Cell 149 (5) (2012) 1060–1072.
[14] S.J. Dixon, D.N. Patel, M. Welsch, R. Skouta, E.D. Lee, M. Hayano, A.G. Thomas, C.E. Gleason, N.P. Tatonetti, B.S. Slusher, B.R. Stockwell, Pharmacological inhibition of cystine-glutamate exchange induces endoplasmic reticulum stress and ferroptosis, Elife 3 (2014) e02523.
[15] M. Gao, P. Monian, N. Quadri, R. Ramasamy, X. Jiang, Glutaminolysis and transferrin regulate Ferroptosis, Mol. Cell 59 (2) (2015) 298–308.
[16] C. Louandre, Z. Ezzoukhry, C. Godin, J.C. Barbare, J.C. Maziere, B. Chauffert, A. Galmiche, Iron-dependent cell death of hepatocellular carcinoma cells exposed to sorafenib, Int. J. Cancer 133 (7) (2013) 1732–1742.
[17] X. Sun, X. Niu, R. Chen, W. He, D. Chen, R. Kang, D. Tang, Metallothionein-1G

facilitates sorafenib resistance through inhibition of ferroptosis, Hepatology 64 (2) (2016) 488–500.
[18] J. Bruix, S. Qin, P. Merle, A. Granito, Y.H. Huang, G. Bodoky, M. Pracht, O. Yokosuka, O. Rosmorduc, V. Breder, R. Gerolami, G. Masi, P.J. Ross, T. Song, J.P. Bronowicki, I. Ollivier-Hourmand, M. Kudo, A.L. Cheng, J.M. Llovet, R.S. Finn, M.A. LeBerre, A. Baumhauer, G. Meinhardt, G. Han, R. Investigators, Regorafenib for patients with hepatocellular carcinoma who progressed on sorafenib treatment (RESORCE): a randomised, double-blind, placebo-controlled, phase 3 trial, Lancet 389 (10064) (2017) 56–66.
[19] J. Wang, L. Ma, W. Weng, Y. Qiao, Y. Zhang, J. He, H. Wang, W. Xiao, L. Li, Q. Chu, Q. Pan, Y. Yu, F. Sun, Mutual interaction between YAP and CREB promotes tumorigenesis in liver cancer, Hepatology 58 (3) (2013) 1011–1020.
[20] J. Wang, X. Tang, W. Weng, Y. Qiao, J. Lin, W. Liu, R. Liu, L. Ma, W. Yu, Y. Yu, Q. Pan, F. Sun, The membrane protein melanoma cell adhesion molecule (MCAM) is a novel tumor marker that stimulates tumorigenesis in hepatocellular carcinoma, Oncogene 34 (47) (2015) 5781–5795.
[21] X. Zhang, F. Sun, Y. Qiao, W. Zheng, Y. Liu, Y. Chen, Q. Wu, X. Liu, G. Zhu, Y. Chen, Y. Yu, Q. Pan, J. Wang, TFCP2 is required for YAP-dependent transcription to stimulate liver malignancy, Cell Rep. 21 (5) (2017) 1227–1239.
[22] J. Wang, X. Liu, H. Wu, P. Ni, Z. Gu, Y. Qiao, N. Chen, F. Sun, Q. Fan, CREB up-regulates long non-coding RNA, HULC expression through interaction with microRNA-372 in liver cancer, Nucleic Acids Res. 38 (16) (2010) 5366–5383.
[23] G.P. Drummen, L.C. van Liebergen, J.A. Op den Kamp, J.A. Post, C11-BODIPY(581/591), an oxidation-sensitive fluorescent lipid peroxidation probe: (micro)spectroscopic characterization and validation of methodology, Free Radic. Biol. Med. 33 (4) (2002) 473–490.
[24] M. Hayano, W.S. Yang, C.K. Corn, N.C. Pagano, B.R. Stockwell, Loss of cysteinyl-tRNA synthetase (CARS) induces the transsulfuration pathway and inhibits ferroptosis induced by cystine deprivation, Cell Death Differ. 23 (2) (2016) 270–278.
[25] M. Luo, L. Wu, K. Zhang, H. Wang, T. Zhang, L. Gutierrez, P. D O'Connell, Y. Zhang, T. Li, W. Gao, Y.Y. Ren, miR-137 regulates ferroptosis by targeting glutamine transporter SLC1A5 in melanoma, Cell Death Differ. 25 (8) (2018) 1457–1472.
[26] S. Doll, B. Proneth, Y.Y. Tyurina, E. Panzilius, S. Kobayashi, I. Ingold, M. Irmler, J. Beckers, M. Aichler, A. Walch, H. Prokisch, D. Trumbach, G. Mao, F. Qu, H. Bayir, J. Fullekrug, C.H. Scheel, W. Wurst, J.A. Schick, V.E. Kagan, J.P. Angeli, M. Conrad, ACSL4 dictates ferroptosis sensitivity by shaping cellular lipid composition, Nat. Chem. Biol. 13 (1) (2017) 91–98.
[27] H. Yuan, X. Li, X. Zhang, R. Kang, D. Tang, Identification of ACSL4 as a biomarker and contributor of ferroptosis, Biochem. Biophys. Res. Commun. 478 (3) (2016) 1338–1343.
[28] K. Li, R.J. Cao, X.J. Zhu, X.Y. Liu, L.Y. Li, S.S. Cui, Erythropoietin attenuates the apoptosis of adult neurons after brachial plexus root avulsion by downregulating JNK phosphorylation and c-Jun expression and inhibiting c-PARP cleavage, J. Mol. Neurosci. 56 (4) (2015) 917–925.
[29] X. Chen, W. Li, J. Ren, D. Huang, W.T. He, Y. Song, C. Yang, W. Li, X. Zheng, P. Chen, J. Han, Translocation of mixed lineage kinase domain-like protein to plasma membrane leads to necrotic cell death, Cell Res. 24 (1) (2014) 105–121.
[30] H. Wang, L. Sun, L. Su, J. Rizo, L. Liu, L.F. Wang, F.S. Wang, X. Wang, Mixed lineage kinase domain-like protein MLKL causes necrotic membrane disruption upon phosphorylation by RIP3, Mol. Cell 54 (1) (2014) 133–146.
[31] S. Buren, A.L. Gomes, A. Teijeiro, M.A. Fawal, M. Yilmaz, K.S. Tummala, M. Perez, M. Rodriguez-Justo, R. Campos-Olivas, D. Megias, N. Djouder, Regulation of OGT by URI in response to glucose confers c-MYC-dependent survival mechanisms, Cancer Cell 30 (2) (2016) 290–307.
[32] K. Guo, L. Gan, S. Zhang, F.J. Cui, W. Cun, Y. Li, N.X. Kang, M.D. Gao, K.Y. Liu, Translocation of HSP27 into liver cancer cell nucleus may be associated with phosphorylation and O-GlcNAc glycosylation, Oncol. Rep. 28 (2) (2012) 494–500.
[33] H. Qiu, F. Liu, T. Tao, D. Zhang, X. Liu, G. Zhu, Z. Xu, R. Ni, A. Shen, Modification of p27 with O-linked N-acetylglucosamine regulates cell proliferation in hepatocellular carcinoma, Mol. Carcinog. 56 (1) (2017) 258–271.
[34] Q. Liu, T. Tao, F. Liu, R. Ni, C. Lu, A. Shen, Hyper-O-GlcNAcylation of YB-1 affects Ser102 phosphorylation and promotes cell proliferation in hepatocellular carcinoma, Exp. Cell Res. 349 (2) (2016) 230–238.
[35] K. Raychaudhuri, N. Chaudhary, M. Gurjar, R. D'Souza, J. Limzerwala, S. Maddika, S.N. Dalal, 14-3-3sigma gene loss leads to activation of the epithelial to mesenchymal transition due to the stabilization of c-Jun protein, J. Biol. Chem. 291 (31) (2016) 16068–16081.
[36] B.R. Stockwell, J.P. Friedmann Angeli, H. Bayir, A.I. Bush, M. Conrad, S.J. Dixon, S. Fulda, S. Gascon, S.K. Hatzios, V.E. Kagan, K. Noel, X. Jiang, A. Linkermann, M.E. Murphy, M. Overholtzer, A. Oyagi, G.C. Pagnussat, J. Park, Q. Ran, C.S. Rosenfeld, K. Salnikow, D. Tang, F.M. Torti, S.V. Torti, S. Toyokuni, K.A. Woerpel, D.D. Zhang, Ferroptosis: a regulated cell death Nexus linking metabolism, redox biology, and disease, Cell 171 (2) (2017) 273–285.
[37] S. Torii, R. Shintoku, C. Kubota, M. Yaegashi, R. Torii, M. Sasaki, T. Suzuki, M. Mori, Y. Yoshimoto, T. Takeuchi, K. Yamada, An essential role for functional lysosomes in ferroptosis of cancer cells, Biochem. J. 473 (6) (2016) 769–777.
[38] G. Wu, Y.Z. Fang, S. Yang, J.R. Lupton, N.D. Turner, Glutathione metabolism and its implications for health, J. Nutr. 134 (3) (2004) 489–492.
[39] E. Mullarky, L.L. Lairson, L.C. Cantley, C.A. Lyssiotis, A novel small-molecule inhibitor of 3-phosphoglycerate dehydrogenase, Mol Cell Oncol 3 (4) (2016) e1164280.
[40] X. Sun, Z. Ou, R. Chen, X. Niu, D. Chen, R. Kang, D. Tang, Activation of the p62-Keap1-NRF2 pathway protects against ferroptosis in hepatocellular carcinoma cells, Hepatology 63 (1) (2016) 173–184.
[41] W. Chen, W. Xiao, K. Zhang, X. Yin, J. Lai, L. Liang, D. Chen, Activation of c-Jun predicts a poor response to sorafenib in hepatocellular carcinoma: preliminary clinical evidence, Sci. Rep. 6 (2016) 22976.
[42] Y. Haga, T. Kanda, M. Nakamura, S. Nakamoto, R. Sasaki, K. Takahashi, S. Wu, O. Yokosuka, Overexpression of c-Jun contributes to sorafenib resistance in human hepatoma cell lines, PLoS One 12 (3) (2017) e0174153.
[43] M.J. Lukey, K.S. Greene, J.W. Erickson, K.F. Wilson, R.A. Cerione, The oncogenic transcription factor c-Jun regulates glutaminase expression and sensitizes cells to glutaminase-targeted therapy, Nat. Commun. 7 (2016) 11321.